ACS APPLIED MATERIALS & INTERFACES

www.acsami.org

Research Article

Photoelectrochemical IL-6 Immunoassay Manufactured on Multifunctional Catecholate-Modified TiO_2 Scaffolds

Sadman Sakib, Amin Hosseini, Igor Zhitomirsky,* and Leyla Soleymani*

Cite This: *ACS Appl. Mater. Interfaces* 2021, 13, 50851−50861

Read Online

ACCESS | Metrics & More | Article Recommendations | Supporting Information

ABSTRACT: There is an increasing interest in using photoelectrochemistry for enhancing the signal-to-noise ratio and sensitivity of electrochemical biosensors. Nevertheless, it remains challenging to create photoelectrochemical biosensors founded on stable material systems that are also easily biofunctionalized for sensing applications. Herein, a photoelectrochemical immunosensor is reported, in which the concentration of the target protein directly correlates to a change in the measured photocurrent. The material system for the photoelectrode signal transducer involves using catecholate ligands to modify the properties of TiO_2 nanostructures in a three-pronged approach of morphology tuning, photoabsorption enhancement, and facilitating bioconjugation. The catecholate-modified TiO_2 photoelectrode is combined with a signal-off direct immunoassay to detect interleukin-6 (IL-6), a key biomarker for diagnosing and monitoring various diseases. Catecholate ligands are added during hydrothermal synthesis of TiO_2 to enable the growth of three-dimensional nanostructures to form highly porous photoelectrodes that provide a three-dimensional scaffold for immobilizing capture antibodies. Surface modification by catecholate ligands greatly enhances photocurrent generation of the TiO_2 photoelectrodes by improving photoabsorption in the visible range. Additionally, catecholate molecules facilitate bioconjugation and probe immobilization by forming a Schiff-base between their −COH group and the $-NH_2$ group of the capture antibodies. The highest photocurrent achieved herein is 8.89 μA cm^{-2}, which represents an enhancement by a factor of 87 from unmodified TiO_2. The fabricated immunosensor shows a limit-of-detection of 3.6 pg mL^{-1} and a log−linear dynamic range of 2−2000 pg mL^{-1} for IL-6 in human blood plasma.

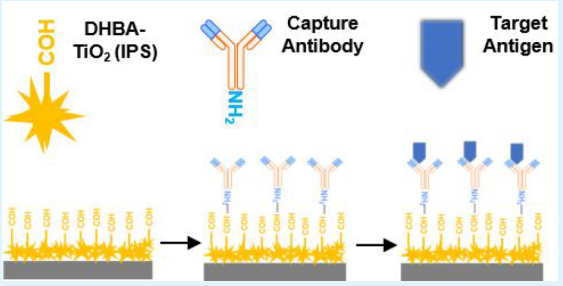

KEYWORDS: *photoelectrochemistry, immunosensor, biosensor, TiO_2, 3D nanostructures, surface modification, catecholate*

INTRODUCTION

Biosensors are devices that couple biorecognition elements with signal transduction mechanisms to quantify and analyze biologically relevant analytes.[1] Research in the field of biosensing is increasingly focusing on improving real-time health monitoring, point-of-care diagnosis, treatment selection, and monitoring of treatment response.[1−5] Recent investigations have highlighted the importance of protein biosensing for the reliable detection of inflammatory processes, autoimmune disorders, cardiovascular disorders, and cancers.[6−9] Among the signal transduction methods used for signal readout in biosensors, photoelectrochemical (PEC) readout has generated tremendous interest due to its low limit-of-detection (LOD),[10] high sensitivity,[3] and broad linear dynamic range.[4] In PEC signal transduction, light and electricity are used as input and output signals, respectively. This decoupling of input and output signals in conjunction with photoamplification strategies allows for the creation of highly sensitive biosensors.[2,3,11] Given the possibility of optical biasing in PEC biosensors, these systems are operated at lower applied electrical potentials compared to their electrochemical counterparts, which reduces the background signals caused by interfering electrochemical signals, thus enhancing the signal-to-background ratio and limit-of-detection of PEC biosensors.[2,3,11] In PEC immunosensors used for protein biosensing, biorecognition occurs on the surface of the photoelectrode, on which photon-enabled electrochemical reactions are measured.[3] It is desirable for photoelectrodes used in PEC biosensing to have high incident photon-to-converted electron efficiency to increase the electrochemical reaction rate and the resultant photocurrent.[3,11]

TiO_2 is commonly used as the photoactive material in PEC biosensing[12−17] due to its high photocatalytic efficiency, chemical stability, tunable morphology, water insolubility, low toxicity, low cost, and ideal conduction and valence band levels for driving electrochemical reactions.[2,18,19] However, unmodified TiO_2 has poor light absorption in the visible

Received: September 22, 2021
Accepted: October 11, 2021
Published: October 19, 2021

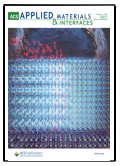

range[12,13] along with high photogenerated charge carrier recombination rate, limiting its photocurrent generation efficiency.[18,19] To overcome these limitations, researchers have employed various photoabsorption and photocurrent amplification strategies that couple TiO_2 with plasmonic noble metal nanoparticles (NP),[20] quantum dots,[21] metal-oxides with different bandgaps,[22] and organic ligands.[23] The surface modification of TiO_2 nanostructures with organic ligands, particularly catecholate ligands, is a very promising photoabsorption and photocurrent amplification strategy due to their strong adsorption onto the surface of metal oxides and the resultant formation of charge transfer complexes.[12,24,25]

The most commonly used TiO_2 structures used in PEC biosensing are nanoparticles due to their high surface area to volume ratio.[2,3,15,18] In spite of this, when TiO_2 nanoparticles are made into films deposited onto photoelectrodes, a large fraction of their surface area is inaccessible due to their compact form factor, thus limiting their interaction with the electrolyte and their available surface area for modification with biorecognition layers. Three dimensional (3D) nanostructures mitigate this problem by forming porous photoelectrodes, through which they improve electrolyte and biomolecular access. Additionally, 3D nanostructures improve photocurrent generation by increasing charge carrier migration and reducing charge recombination rate, since charge carriers are less localized compared to nanoparticles.[3,18,26,27]

Here, we sought to create 3D TiO_2 nanostructures that yielded a porous architecture desirable for biosensing, had enhanced PEC current generation in the visible light compared to unmodified TiO_2 nanostructures, and could be easily functionalized with biorecognition elements for biosensing. For this purpose, we used multifunctional catecholate molecules. Catecholate ligands are known to strongly adsorb onto the surface of TiO_2.[12,28,29] As such, researchers have demonstrated that surface modification of TiO_2 nanostructures with catecholate ligands is an excellent photoexcitation enhancement strategy.[12,30−32] The TiO_2−catecholate ligand complex is utilized in various applications such as PEC biosensing,[12,13] water splitting,[30,32,33] solar cells,[34−36] and photocatalytic pollutant degradation.[37−39] Previous studies have primarily focused on enhancing the photoexcitation of the TiO_2-catecholate ligand complex by adding catecholate ligands to presynthesized TiO_2 nanostructures. The formation and performance of TiO_2−catecholate complexes is influenced by the chemical structure of the catecholate molecules. The chemical properties and electric charge of the functional groups of catecholate ligands influence their solubility, adsorption on TiO_2 particles, strength as dispersing agents, photovoltaic performance of the complexes, and their interactions with other components of the biosensors. As such, in situ modification of TiO_2 using catecholates as capping and dispersing agents for synthesis is promising for tuning the morphology and properties of TiO_2 structures. The goal of this work was to take advantage of the strong surface adsorption property of catecholate ligands to tune the morphology of TiO_2 during synthesis to produce 3D TiO_2 nanostructures that were able to form highly porous photoelectrodes. The catecholate surface modification was also hypothesized to enhance photocurrent generation in the 3D TiO_2 nanostructures by improving photoabsorption and charge. Lastly, the functional groups on the catecholate molecules would allow facile functionalization of the photoelectrodes with biorecognition elements.

The developed 3D TiO_2 photoelectrodes were functionalization with biorecognition elements for creating a biosensor for analyzing interleukin-6 (IL-6), a biomarker with key roles in immunomodulation, hematopoiesis, and inflammation processes in the human body. IL-6 levels in the body are linked to several cancers and diseases such as meningitis, Alzheimer's disease, rheumatoid arthritis, lymphoma, myeloma, or psoriasis.[40−42] The results presented below reveal key insights into development of new material systems for the fabrication of high performance PEC biosensors.

RESULTS AND DISCUSSION

With the purpose of creating 3D TiO_2 nanostructures, we explored the addition of catecholate molecules during the acid-hydrothermal synthesis of TiO_2. 3,4-Dihydroxybenzaldehyde (DHBA) and caffeic acid (CA) were the catecholate molecules used for the TiO_2 synthesis process (Figure 1A). The common

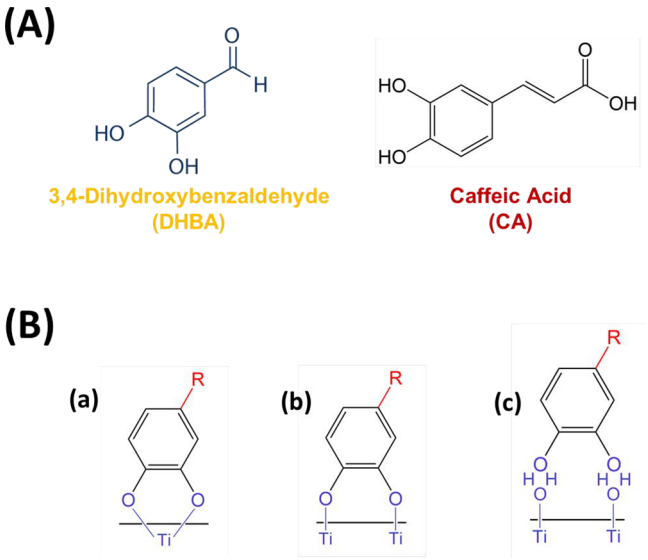

Figure 1. (A) Chemical structures of catecholate molecules used for modifying TiO_2, (B) bonding mechanisms of a catechol group to TiO_2 surface: (a) bidentate chelating, (b) bidentate bridging (inner sphere), and (c) bidentate bridging (outer sphere) bonding of catechol group. R group represents −CH−CH−COOH for CA and −COH for DHBA.

structural features shared by catecholate molecules is the presence of an aromatic ring with two adjacent phenolic −OH groups. The chemical structures of the molecules also included a short hydrocarbon chain that ends in various functional groups. In the case of DHBA and CA, their hydrocarbon chains end in −COH and −COOH groups, respectively.[28,29] Catecholate ligands readily adsorb onto the surface of metal oxide particles via bidentate bonding (Figure 1B).[12,28,29] In this bonding mechanism, surface Gibbs energy is minimized when adsorbed water molecules dissociate to produce a hydroxylated surface. The bidentate type bonding occurs via the surface adsorption process, when two adjacent phenolic −OH groups are deprotonated and coordinate with the metal cation through dehydration of the surface hydroxyl groups or by outer sphere bonding.[43−45]

Seven different TiO_2 nanostructures were synthesized using a standard acid-hydrothermal synthesis procedure[46] and CA or DHBA was added in situ to observe changes in the

https://doi.org/10.1021/acsami.1c18240
ACS Appl. Mater. Interfaces 2021, 13, 50851−50861

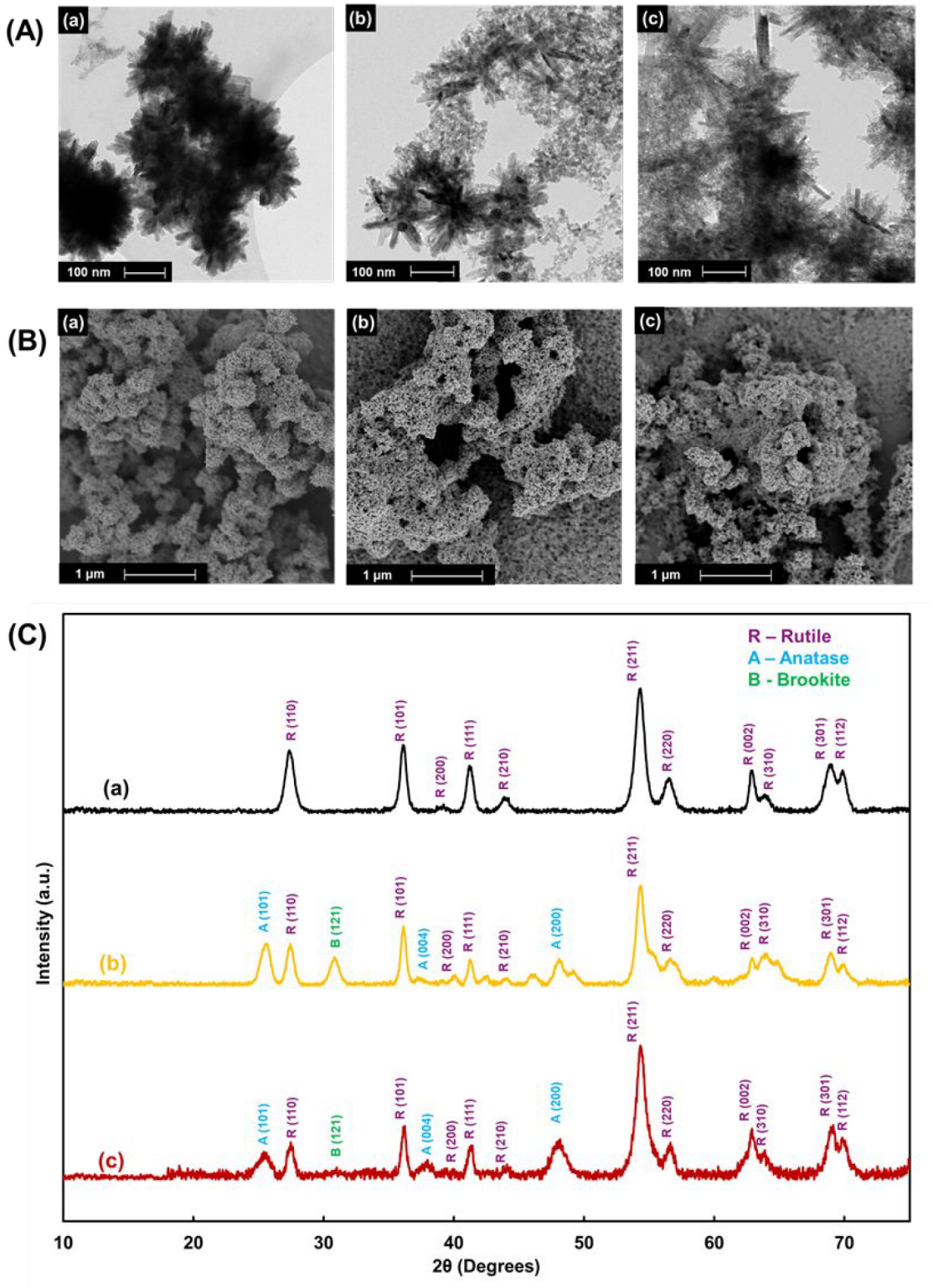

Figure 2. (A) TEM images of synthesized TiO_2 nanostructures. (B) SEM images of synthesized TiO_2 nanostructures deposited onto ITO-PET substrate. (C) XRD data of acid-hydrothermally synthesized TiO_2 nanostructures (a) bare TiO_2, (b) DHBA-TiO_2 (IS), and (c) CA-TiO_2 (IS).

morphology and PEC response of the nanostructures: bare TiO_2, CA-TiO_2 (IS), DHBA-TiO_2 (IS), CA-TiO_2 (PS), DHBA-TiO_2 (PS), CA-TiO_2 (IPS), and DHBA-TiO_2 (IPS). Bare TiO_2 refers to the unmodified sample that did not have any catecholate molecules added during or after the synthesis process. CA-TiO_2 (IS) and DHBA-TiO_2 (IS) refer to samples that had CA or DHBA added during synthesis. CA-TiO_2 (PS) and DHBA-TiO_2 (PS) are samples that were first synthesized as the bare TiO_2, but had CA or DHBA added to them after synthesis. Lastly, the CA-TiO_2 (IPS) and DHBA-TiO_2 (IPS) samples had CA or DHBA added *both* during and after synthesis. The bare TiO_2 were composed of aggregated nanorods that radially extended outward; whereas, the CA-TiO_2 (IS) and DHBA-TiO_2 (IS) were made of more loosely

https://doi.org/10.1021/acsami.1c18240
ACS Appl. Mater. Interfaces 2021, 13, 50851−50861

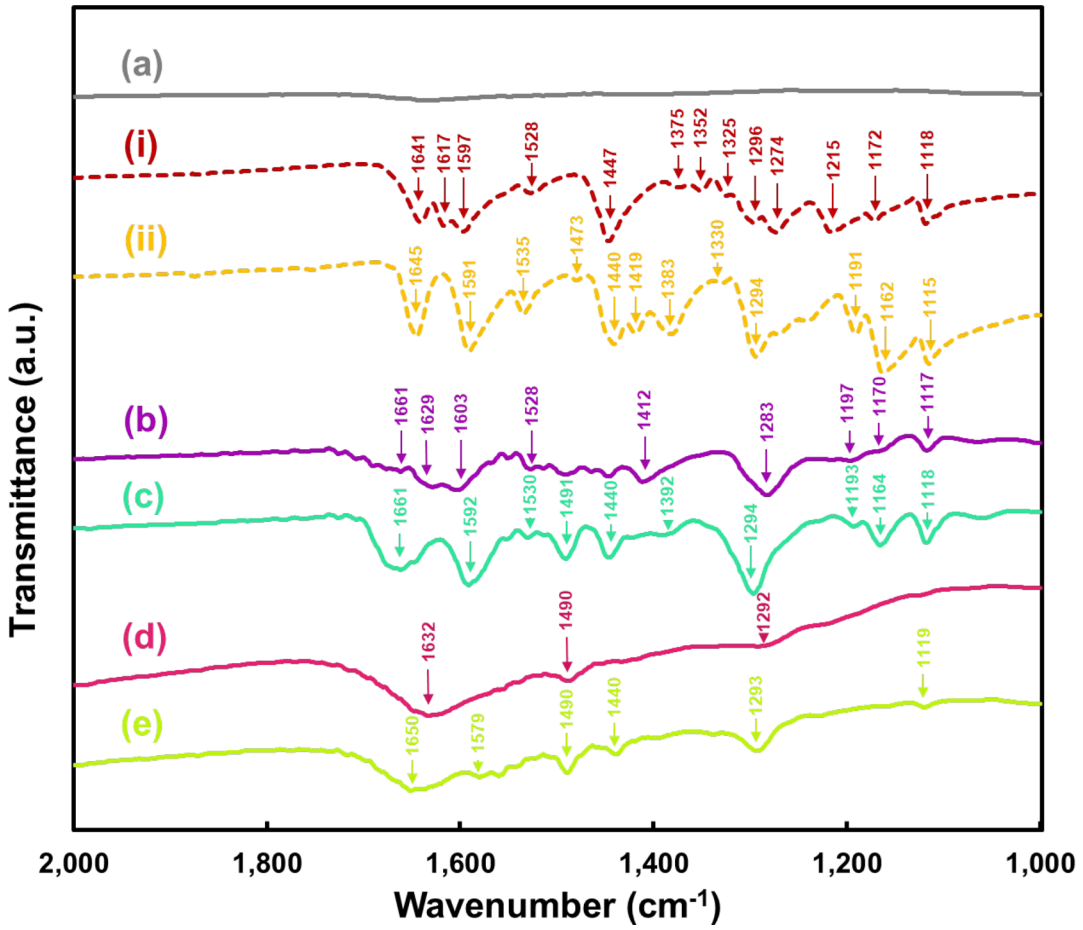

Figure 3. FTIR spectroscopy data for (a) bare TiO_2, (b) CA-TiO_2 (PS), (c) DHBA-TiO_2(PS), (d) CA-TiO_2 (IS), and (e) DHBA-TiO_2 (IS). (i) and (ii) are CA and DHBA, respectively.

packed nanorods and were surrounded by nanoparticles (Figure 2A). These new morphologies are attributed to DHBA and CA readily adsorbing onto the surface of TiO_2 nanostructures as they form, stabilizing their surface to prevent aggregation. When the TiO_2 nanostructures are deposited onto a planar substrate they form a nanoporous surface, as shown by SEM imaging (Figure 2B). As shown in the XRD data, both the CA-TiO_2 (IS) and DHBA-TiO_2 (IS) predominantly contain the rutile phase, with small amounts of anatase and a negligible amount of brookite phase impurities (Figure 2C). The shape of the diffraction peaks suggests that all the synthesized particles have high crystallinity; however, the CA-TiO_2 (IS) and DHBA-TiO_2 (IS) showed lower crystallinity than the unmodified particles. With the addition of surfactants that have preferential binding affinity for specific crystal facets, it is possible to control the growth of TiO_2 nanostructures during synthesis.[47−49] On the basis of density functional theory models, catecholate ligands are known to preferentially adsorb onto the {110} facet of rutile TiO_2.[25] It is proposed that CA and DHBA, preferentially adsorb onto the {110} facet of TiO_2 during acid-hydrothermal synthesis, preventing further growth. This encourages anisotropic growth of TiO_2 on other crystal facets with high surface energies. This is supported by the XRD data, where we see that the {211} diffraction of peak of the CA-TiO_2 and DHBA-TiO_2 are higher than the {110} diffraction peaks, whereas the opposite is the case for the bare TiO_2.

The expected bidentate bonding of catecholate molecules to metal oxides was evaluated using FTIR spectroscopy (Figure 3) for a subset of the above-mentioned nanostructures. In the wavenumber range of 1000−2000 cm^{-1}, bare TiO_2 does not have any discernible peaks; however, CA and DHBA show several peaks. These CA and DHBA peaks were also observed in the CA-TiO_2 (PS) and DHBA-TiO_2 (PS) samples, with minor shifting. It was also observed that the peaks related to C−O stretching and bending (1528, 1597, and 1296 cm^{-1} are intensified, while other peaks are reduced. This indicates the formation of bidentate-type bonding between TiO_2 and CA/DHBA. In the CA-TiO_2 (IS) and DHBA-TiO_2 (IS) samples, most peaks not related to C−O stretching and bending are significantly reduced compared to bare TiO_2 suggesting that the surface adsorbed CA and DHBA may be partially decomposed during synthesis after binding to the surface of TiO_2.

All the TiO_2 nanostructures, modified with catecholate molecules during or after synthesis, were optically and photoelectrochemically characterized (Figure 4). For bare TiO_2, we observe excellent light absorption in the UV range (<380 nm) and poor light absorption in the visible range (380−700 nm) (Figure 4A). The UV/vis spectroscopy confirms that all TiO_2 nanostructures with the catecholate surface modification show significantly enhanced absorption in both the visible range and the near UV range, compared to the bare TiO_2. Adsorption of catecholate ligands on the surface of TiO_2 forms charge transfer complexes that greatly improve

https://doi.org/10.1021/acsami.1c18240
ACS Appl. Mater. Interfaces 2021, 13, 50851−50861

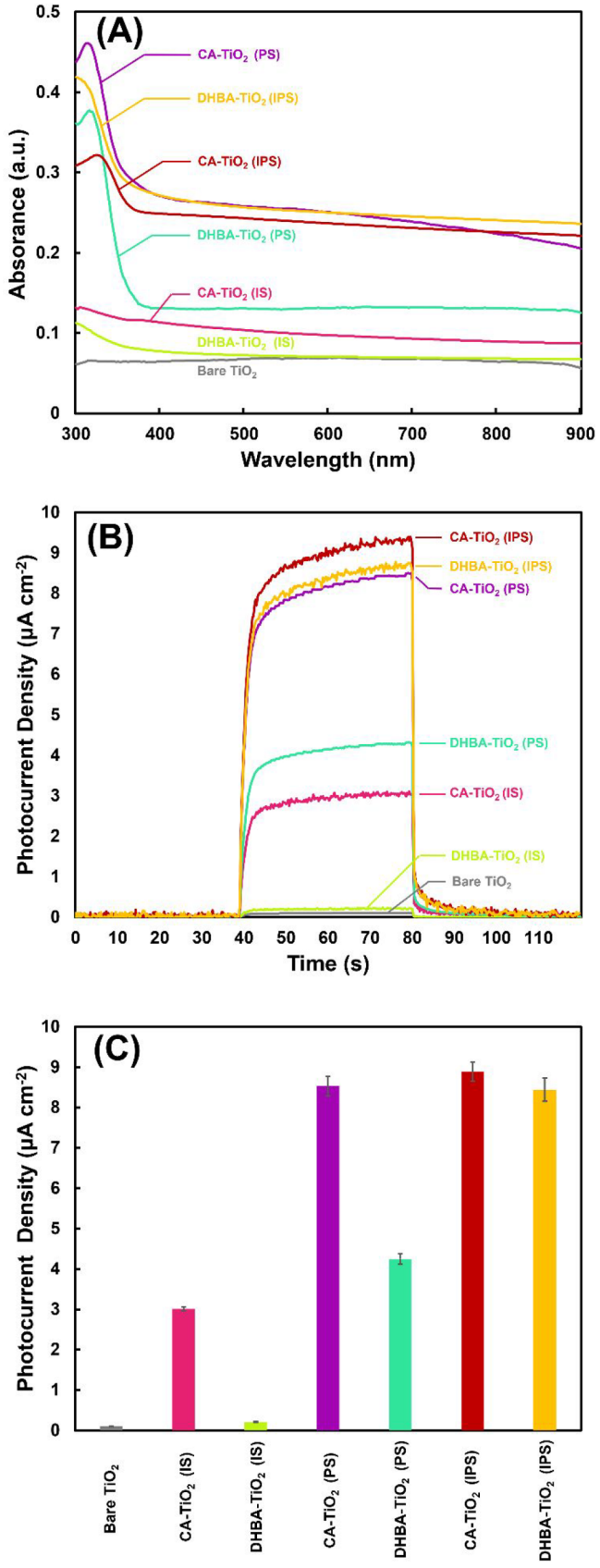

Figure 4. Optical and photoelectrochemical characterization of TiO_2 nanostructures. (A) UV/visible absorbance spectroscopy of TiO_2 nanostructures. (B) Chronoamperometric curves of TiO_2 nanostructures with and without optical illumination. (C) Summary of photocurrent densities for various TiO_2 nanostructures. The bars represent the mean value obtained from at least three separate electrodes, with the error bars representing the standard deviation. The photocurrent measurements were performed at 0 V potential vs Ag/AgCl using 0.1 M ascorbic acid in 0.1 M PBS as the electrolyte. The photoelectrodes were irradiated with white light and the average photocurrent density was measured by taking the running average of the last 10 s of the irradiation period.

light absorption in the visible and the near UV range by facilitating improved photoexcited electron injection into the TiO_2 conduction band.[32,50,51] Photocurrent measurements were performed by exciting the TiO_2 photoelectrodes using white light (Figure 4C). Photons with energies high enough to overcome the TiO_2 bandgap generate electron−hole pairs. The holes in the valence band oxidize ascorbic acid at the electrode/electrolyte interface, generating an anodic photocurrent.[52,53] The photocurrent density of the TiO_2 nanostructures when ordered from highest to lowest are CA-TiO_2(IPS) > CA-TiO_2(PS) > DHBA-TiO_2(IPS) > DHBA-TiO_2(PS) > CA-TiO_2(IS) > DHBA-TiO_2(IS) > bare TiO_2. The sample with the highest photocurrent is CA-TiO_2 (IPS) at 8.89 μA cm^{-2}, which demonstrates an enhancement by a factor of 87 from bare TiO_2. CA-modified TiO_2 had higher photocurrents compared to their DHBA-modified counterparts. This is consistent with our previous experiments,[12] where it was shown that catecholate ligands with longer hydrocarbon tails demonstrate a larger photocurrent enhancement. The IS samples demonstrate lower photocurrents compared to the PS or IPS samples. The IPS samples slightly outperform PS samples, which can be explained by their crystalline composition. Based on the XRD data (Figure 2C), IPS samples contain both rutile and anatase phases, whereas the PS samples only contain the rutile phase. The combination of rutile (~3.0 eV) and anatase (~3.2 eV) phases improves the photocurrent of IPS samples via dual sensitization. Coupling large bandgap and small bandgap semiconductors results in a multistaged bandgap that improves electron−hole pair generation efficiency by allowing lower energy photons to excite the system; this process results in improved absorbance in the visible range.[54−56]

It has been reported that 3D metal-oxide nanostructures such as nanorod arrays,[57] nanoflowers,[58] and mesoporous films[59] demonstrate higher charge carrier separation, reduced charge carrier recombination rate, and lower charge transfer resistance, compared to their NP counterparts.[22,60] This has been attributed to the increased length-scale of 3D nanostructures, which provides a "highway" for charge transport along their longitudinal direction.[22,61] 3D nanostructures also boast higher light absorption than NP morphologies due to increased internal light scattering.[22,57] All of these qualities generally endow 3D nanostructured metal oxides with enhanced photocurrent generation over metal oxide NP. The observed surfaces in Figure 2B have a similar morphology to the 3D nanostructured metal oxides found in literature and are expected to have similar photocurrent generation enhancement. Additionally, it has been reported that 3D nanostructured electrodes can increase the sensitivity of a biosensor by a 100-fold compared to their planar counterparts made from nanoparticles.[62−64] The use of 3D nanostructures gives photoelectrodes a higher electroactive surface area compared to planar photoelectrodes of the same footprint, which in turn

https://doi.org/10.1021/acsami.1c18240
ACS Appl. Mater. Interfaces 2021, 13, 50851−50861

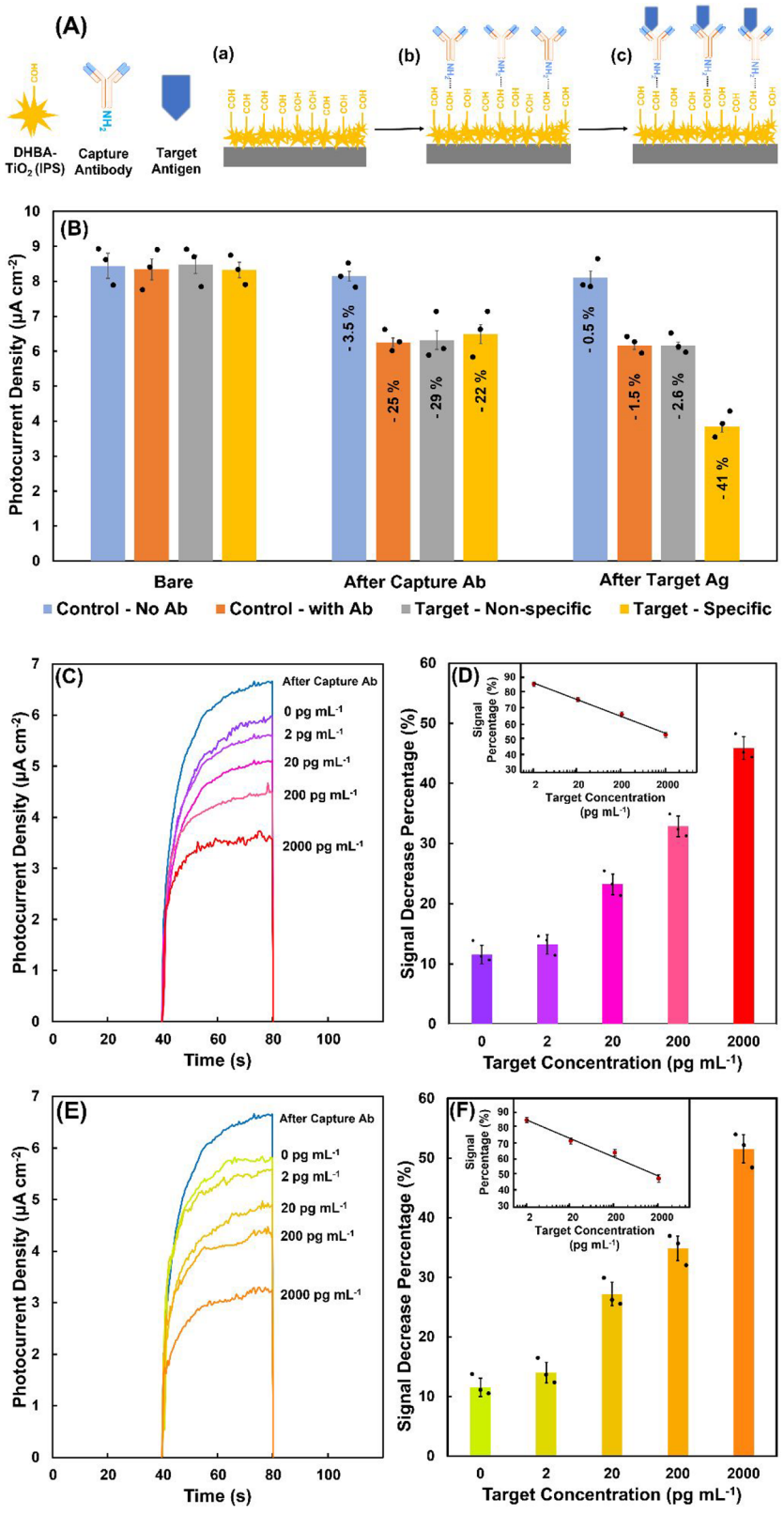

Figure 5. Characterization of the PEC immunoassay (A) Fabrication of the signal-off immunoassay: (a) deposition of DHBA-TiO_2 (IPS) on the substrate (b) modification with capture antibody and (c) complexation with target protein. (B) Photocurrent density of DHBA-TiO_2 (IPS) photoelectrodes at bare, probe immobilization, and target capture stages of immunosensor operation in buffer. (C) PEC curves demonstrating the signal response at various target concentrations in buffer. (D) Photocurrent signal decrease at various IL-6 concentrations obtained from the PEC immunosensor in buffer. The inset shows a calibration curve with the data points fitted to a line by equation $S = 10.76 \times \log C + 9.43$ and with $R^2 = 0.99$. (E) PEC curves demonstrating the signal response at various target concentrations in 20% human blood plasma. (F) Photocurrent signal decrease at various IL-6 concentrations ontained from the PEC immunosensor in 20% human blood plasma. The inset shows a calibration curve with the data points fitted to a line by equation $S = 12.02 \times \log C + 10.25$ and with $R^2 = 0.98$.

https://doi.org/10.1021/acsami.1c18240
ACS Appl. Mater. Interfaces 2021, 13, 50851−50861

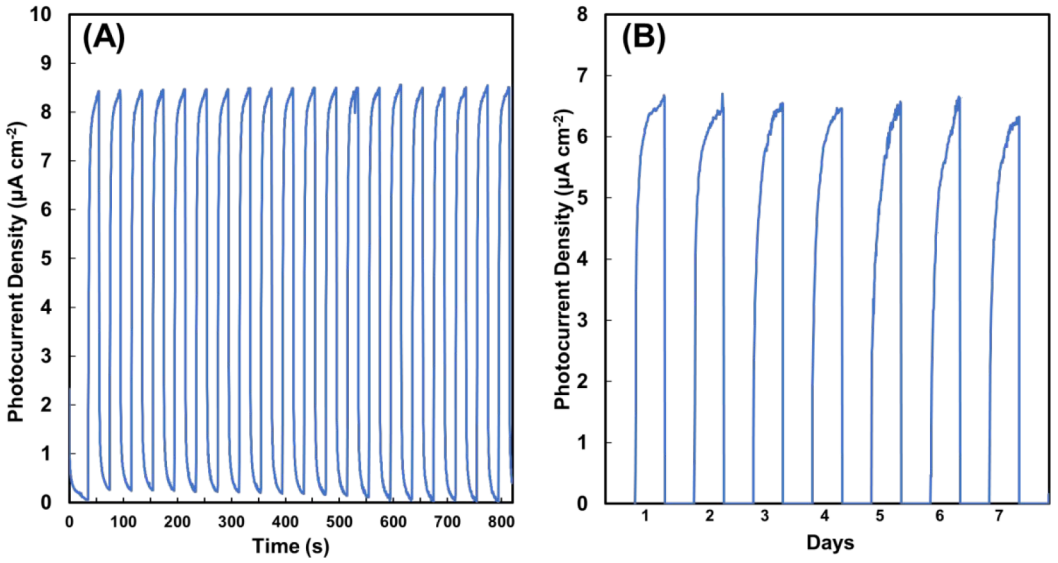

Figure 6. Evaluation of the stability of the PEC biosensor. (A) Photocurrent density measurements for 20 continuous cycles of the bare DHBA-TiO_2 (IPS) photoelectrodes. (B) Photocurrent density measurements following the storage of capture antibody modified DHBA-TiO_2 (IPS) photoelectrodes for 7 days.

increases the probe molecule immobilization density and the target capture density.[62−64] The photocurrent enhancement, solely attributed to the physical features of the nanostructures, could not be directly quantified here due to the presence of photoabsorption enhancing catecholate ligands. The DHBA-TiO_2 (IPS) nanostructures were used for the creation of PEC biosensors due to their high photocurrent and the presence of −COH group on their surface that can react with the $-NH_2$ groups of antibodies through Schiff-base reactions. The PEC biosensor is created by immobilizing anti-IL6 capture antibodies on the photoelectrode, which can then bind to the target IL-6 antigen (Figure 5A). It is expected that in the presence of IL-6, the measured photoelectrochemical current would decrease due to the reduced access of the ascorbic acid to the electrode surface. Other 3D nanostructured electrodes composed of nanorod arrays,[57,65,66] nanoflakes,[58,67,68] and mesoporous films[59] (Supporting Information, SI, Table S1), have been reported in the literature for PEC applications. These 3D nanostructured electrodes are generally made from metal oxides such as TiO_2, ZnO, and BiOI.[60] Some of these structures also include functionalization with other photoactive materials such as plasmonic NPs, quantum dots, and other metal oxide nanoparticles as part of a broader photoexcitation enhancement strategy.[20−22,60] Hydrothermal synthesis is the most common method for fabricating these 3D nanostructured photoelectrodes, followed by chemical vapor deposition, electrodeposition, and successive ionic layer adsorption and reaction. However, all of these fabrication methods require initial seeding of a substrate with a precursor structure to create the 3D nanostructuring.[60] This makes the fabrication of 3D nanostructured electrodes highly inefficient, lengthy, and costly, as the production is limited by the geometric area of the substrate able to fit inside the instrument used for synthesis. The synthesis method presented in this work does not suffer from such a drawback. Acid-hydrothermal synthesis of TiO_2 combined catecholate-induced morphology tuning can produce hierarchical 3D TiO_2 nanostructures without the need for substrate seeding, resulting in high volume and high concentration suspensions of 3D nanostructures.

In order to validate each step involved in the development of the PEC biosensor, we measured the photocurrent before and after each step in buffer solution, and quantified the signal change caused as a result (Figure 5B). The immobilization of probe antibodies on the photoelectrodes resulted in a signal decrease (−22% to −29%) for all the data sets, that was significantly larger in magnitude compared to the observed signal decrease with a blank solution that did not contain any antibody (−3%). This indicated the successful biofunctionalization of the photoelectrode. The immobilization of the capture antibody decreases the photocurrent by limiting the access of ascorbic acid from the electrolyte to the photoelectrode surface.[69,70] Incubation with the specific target IL-6 demonstrated a significantly larger signal change (−41%) compared to incubation with the nonspecific target (−3%), bovine serum albumin (BSA), and the blank (−1%) solution, demonstrating the ability of the PEC sensor in detecting the specific target. Target complexation results in further steric hindrance leading to more signal decrease. In order to determine the analytical performance of the PEC biosensor, we assessed it with logarithmically increasing IL-6 concentrations in buffer (Figure 5C,D) and 20% human blood plasma, ranging from 2−2000 pg mL^{-1} (Figure 5E,F). As expected, the PEC current decreased in magnitude with increasing target concentration in both mediums (Figure 5D,F), and the percentage change in PEC current increased in magnitude with increasing the target concentration. The signal decrease measured in plasma was in good agreement with that measured in buffer, demonstrating negligible signal change due to biofouling (<6%). The sensor demonstrated a log−linear operational range of 2−2000 pg mL^{-1}, with a limit-of-detection (LOD) of 3.6 pg mL^{-1} in plasma and 1.6 pg mL^{-1} in buffer solution.

The short-term stability of the sensor was evaluated by measuring the photocurrent density for 20 continuous cycles for bare DHBA-TiO_2(IPS) photoelectrodes (Figure 6A), demonstrating negligible scan-to-scan variability (signal change of 0.86% over 20 scans and 14 min). The long-term stability was evaluated by storing capture antibody modified photo-

https://doi.org/10.1021/acsami.1c18240
ACS Appl. Mater. Interfaces 2021, 13, 50851−50861

electrodes over a period of 7 days and measuring the photocurrent density each day (Figure 6B). The sensor demonstrates good long-term stability, with a ~6% signal decrease after 7 days.

The above data makes it evident that catecholate surface modified TiO_2 nanostructures, specifically DHBA-TiO_2 (IPS), are an excellent material system for use in PEC biosensors with a wide dynamic range and a low LOD. Some recent examples for PEC IL-6 biosensors in literature include TiO_2 nanoparticles dual cosensitized with CdS and CdSe on ITO electrodes (LOD = 0.38 pg mL^{-1}, dynamic range = 0.1−1 pg mL^{-1}),[14] and the use of perovskite-type $LaFeO_3$ nanoparticles deposited on fluorine-doped tin oxide electrodes (LOD = 33 fg mL^{-1}, dynamic range = 0.1−100 pg mL^{-1}).[71] The main advantage offered by our system is its wide dynamic range which covers the diagnostic IL-6 concentration range of diseases such as Alzheimer's disease (85−567 pg mL^{-1}), rheumatoid arthritis (17 pg mL^{-1}), myocardial infraction (28.5−46.5 pg mL^{-1}), cachexia (100 pg mL^{-1}), cardiac myxoma (>56 pg mL^{-1}), multiple myeloma (5−33 pg mL^{-1}), hepatocyte carcinoma (7−18.9 pg mL^{-1}), and Burkitt lymphoma (100.3 pg mL^{-1}),[40] while still maintaining clinically acceptable LOD and stability. Commercial IL-6 biosensors (SI Table S2) are typically based on enzyme-linked immunosorbent assays (ELISA).[72] These commercial devices rely on chemiluminescence,[73] electrochemiluminescence,[74] or colorimetry[75] as their principle signal transduction mechanism, which require the use of benchtop plate readers. The LOD of these assays range from 0.2 to 5 pg/mL putting the LOD of our device (3.6 pg/mL) well within this range. In contrast to the above-mentioned assays, our newly developed system does not require target labeling, which reduces the number of steps required for assay operation. Furthermore, it would be possible in the future to integrate the assay with hand-held and portable signal readers for point-of-care analysis.

CONCLUSIONS

In this work, we developed an advanced material synthesis process to create photoelectrodes for use in photoelectrochemical biosensors. These photoelectrodes use catecholate-modified TiO_2 nanostructures to provide a 3D architecture, enhanced photoelectrochemical response, and functional ligands for effective biofunctionalization. The chemical structure of the selected multifunctional catecholate molecules is a key factor, which governs the material properties and efficient biosensor performance. Compared to photoelectrodes created from unmodified TiO_2, the catecholate-modified electrodes developed here increase the measured photocurrent by about 2 orders of magnitude. These photoelectrodes were easily modified with antibodies, transforming them into biosensors for detecting IL-6. The fabricated biosensors show great performance with a wide dynamic range of 2−2000 pg mL^{-1}, a limit-of-detection of 3.6 pg mL^{-1} in 20% human blood plasma, and good short- and long-term stability. These photoelectrochemical biosensors have the potential to be used in the clinical analysis of Alzheimer's disease, rheumatoid arthritis, myocardial infraction, cachexia, cardiac myxoma, multiple myeloma, hepatocyte carcinoma, and Burkitt lymphoma. The results presented here also provide insights into the development of robust photoactive material systems for the fabrication of high performance PEC biosensors.

EXPERIMENTAL SECTION

Materials. Caffeic acid (CA), 3,4-dihydroxybenzaldehyde (DHBA), titanium(IV) butoxide, and indium tin oxide/poly(ethylene terephthalate) (ITO/PET) substrates (surface resistivity 100 Ω/sq) were purchased from Sigma-Aldrich. Hydrochloric acid (37%) was purchased from Caledon Laboratory Chemicals. Milli-Q grade (18.2 MΩ cm) deionized (DI) water was used for all solution preparation and washing steps.

Acid-Hydrothermal Synthesis of Nanostructured TiO_2. In a Teflon container, 20 mL of the reaction solution was prepared by mixing 1 M HCl with 1 mL of titanium(IV) butoxide. The Teflon container was inserted into an autoclave and placed in an oven for 2 h at 180 °C to prepare TiO_2 nanostructures via hydrothermal synthesis. For samples with in situ surface modification, 0.05 g of CA or DHBA was also added to the reaction solution. After synthesis, the samples were centrifuged six times at 6000 rpm. This was done to remove reaction byproducts and restore neutral pH in the TiO_2 suspension.

Photoelectrode Fabrication. ITO/PET substrates were cut into dimensions of 1.2 × 0.7 cm^2 and a small portion of length was masked with self-adhesive vinyl to preserve electrical contact area. Substrates were subjected to air plasma treatment for 1 min. The substrates were then coated with unmodified TiO_2 or surface modified TiO_2 by dropping 10 μL of 0.66 g/L suspension on the substrate surface and baking them in the oven at 85 °C for 6 min. This process was repeated three times to deposit three layers.

Material Characterization. The morphology of the synthesized nanostructures was analyzed via transmission electron microscopy (TEM) imaging using a Thermo Scientific Talos 200X STEM Microscope. The surface of photoelectrodes fabricated from the nanostructures were analyzed via scanning electron microscope (SEM) imaging using an FEI Magellan 400 FEGSEM Microscope. For SEM imaging the samples were coated with 3 nm thick layer of platinum. Conventional sample preparation was used for both TEM and SEM imaging. A Bruker SMART CCD 600 Diffractometer using a Cu source was used for obtaining X-ray diffraction (XRD) characterization of the synthesized particles. Fourier transform infrared (FTIR) spectroscopy was performed using a Bruker Vertex 70 spectrometer and Ultraviolet/visible (UV/vis) spectroscopy was performed using a Tecan Evo 200 Plate reader.

Photocurrent measurements were caried out using a Zahner CIMPS-QE/IPCE3 Photoelectrochemical Potentiostat. A standard three-electrode cell setup was used with white light as a photoexcitation source. Platinum (Pt) wire was used as the counter electrode, a silver/silver chloride (Ag/AgCl) electrode for the refence electrode and TiO_2 NS or catecholate-modified TiO_2 NS photoelectrodes acted as the working electrodes. The electrolyte solution was composed of 0.1 M phosphate buffered saline (PBS) and 0.1 M ascorbic acid (AA). The photoexcitation source was a Thorlabs MNWHL4 mounted LED, which has a neutral white color temperature (400−700 nm) and an irradiance of 7.7. uW mm^{-2} (see SI Figure S1 for the spectrum of the light source. The photocurrent measurement was done by running the potentiostat in chronopotentiometric mode for 60 s. The potential of the PEC cell was fixed at 0 V, and the working electrode was irradiated with white light at a 20 s interval. Average photocurrent density was measured by taking the running average of the last 10 s of the irradiation period.

Antibody/Antigen Complexation and Target Detection. Photoelectrodes fabricated from DHBA-modified TiO_2 NS with both in situ and post situ modification were used for PEC-based protein detection testing. The immunoassay format utilized was a direct assay that made use of anti-IL-6 as its single capture antibody and IL-6 as the target antigen. After fabricating the photoelectrodes, their photocurrents were measured to obtain the bare signal. In the first step, a 125 μg mL^{-1} solution of capture Ab was prepared from stock by diluting in 1 M PBS. Then, 15 mL of the capture Ab solution was deposited on top of the photoelectrodes and incubated for 24 h at 20 °C. After this incubation period, the photoelectrodes were washed with 1 M PBS. Photocurrent was once again measured at this point to get the after-capture-Ab signal. In the next step, various concen-

https://doi.org/10.1021/acsami.1c18240
ACS Appl. Mater. Interfaces 2021, 13, 50851−50861

trations of the target Ag ranging from 2 to 2000 pg mL^{-1} was prepared by diluting from stock in 1 M PBS. Then, 15 mL of the target Ag solution was deposited on top of the photoelectrode and further incubated for 1 h at 20 °C. The photoelectrodes were washed with 1x Tris-buffered saline (TBS) and again washed with a mixture of 1x TBS and 0.5% v/v Tween20 (TBST). The photocurrent was measured for a final time to obtain the after-target-Ag signal.

Limit of Detection Calculation. A calibration curve was plotted as a function of the photocurrent density and the concentration of the IL-6 target Ag, which was used to complex with the Anti-IL-6 capture Ag immobilized on the photoelectrode. To simulate the effect of nonspecific absorption of nontarget proteins, one of the measurements contained 2000 pg mL^{-1} of bovine serum albumin (BSA), instead of IL-6; this measurement was treated as the blank signal. Limit of blank (LOB) is calculated using the equation:

$$\mathrm{LOB} = I_{\mathrm{black}} + 3 \times \sigma_{\mathrm{blank}}$$

where, σ_{blank} is the standard deviation of the blank signal and the factor 3 is used to calculate the LOD within a 95% confidence interval. The LOD is then calculated from the regression line by substituting the signal (y-value) with the LOB.

■ ASSOCIATED CONTENT

Supporting Information

The Supporting Information is available free of charge at https://pubs.acs.org/doi/10.1021/acsami.1c18240.

Figure S1, spectrum of the photoexcitation source; Table S1, 3D nanostructure photoelectrodes used in photoelectrochemical biosensing; Table 2, examples of commercial IL-6 immunoassays; and additional references (PDF)

■ AUTHOR INFORMATION

Corresponding Authors

Leyla Soleymani − *Department of Engineering Physics, McMaster University, Hamilton L8S 4L7, Canada; School of Biomedical Engineering, McMaster University, Hamilton L8S 4L7, Canada;* orcid.org/0000-0003-4915-2999; Email: leyla.soleymani@gmail.com

Igor Zhitomirsky − *School of Biomedical Engineering and Department of Materials Science and Engineering, McMaster University, Hamilton L8S 4L7, Canada*; Phone: 1-905-525-9140; Email: zhitom@mcmaster.ca

Authors

Sadman Sakib − *Department of Engineering Physics, McMaster University, Hamilton L8S 4L7, Canada*

Amin Hosseini − *School of Biomedical Engineering, McMaster University, Hamilton L8S 4L7, Canada*

Complete contact information is available at: https://pubs.acs.org/10.1021/acsami.1c18240

Author Contributions

The manuscript was written through contributions of all authors. All authors have given approval to the final version of the manuscript.

Notes

The authors declare no competing financial interest.

■ ACKNOWLEDGMENTS

This research was funded by the Natural Sciences and Engineering Research Council of Canada. L.S. is the Canada Research Chair in Miniaturized Biomedical Devices. Scanning Electron Microscopy was performed at the Canadian Centre for Electron Microscopy.

■ REFERENCES

(1) Soleymani, L.; Li, F. Mechanistic Challenges and Advantages of Biosensor Miniaturization into the Nanoscale. *ACS Sensors* **2017**, *2* (4), 458−467, DOI: 10.1021/acssensors.7b00069.

(2) Victorious, A.; Saha, S.; Pandey, R.; Didar, T. F.; Soleymani, L. Affinity-Based Detection of Biomolecules Using Photo-Electrochemical Readout. *Frontiers in Chemistry*; Frontiers Media S.A.: Lausanne, Switzerland, September 11, 2019. DOI: 10.3389/fchem.2019.00617.

(3) Zhao, W. W.; Xu, J. J.; Chen, H. Y. Photoelectrochemical Immunoassays. *Anal. Chem.* **2018**, *90* (1), 615−627.

(4) Zhao, W. W.; Xu, J. J.; Chen, H. Y. Photoelectrochemical DNA Biosensors. *Chem. Rev.* **2014**, *114* (15), 7421−7441.

(5) Metkar, S. K.; Girigoswami, K. Diagnostic Biosensors in Medicine - A Review. *Biocatal. Agric. Biotechnol.* **2019**, *17*, 271−283.

(6) Chikkaveeraiah, B. V.; Bhirde, A. A.; Morgan, N. Y.; Eden, H. S.; Chen, X. Electrochemical Immunosensors for Detection of Cancer Protein Biomarkers. *ACS Nano* **2012**, *6* (8), 6546−6561.

(7) Ronkainen, N. J.; Okon, S. L. Nanomaterial-Based Electrochemical Immunosensors for Clinically Significant Biomarkers. *Materials* **2014**, *7* (6), 4669−4709.

(8) Yáñez-Sedeño, P.; Campuzano, S.; Pingarrón, J. M. Multiplexed Electrochemical Immunosensors for Clinical Biomarkers. *Sensors* **2017**, *17* (5), 965.

(9) Wu, J.; Fu, Z.; Yan, F.; Ju, H. Biomedical and Clinical Applications of Immunoassays and Immunosensors for Tumor Markers. *TrAC, Trends Anal. Chem.* **2007**, *26* (7), 679−688.

(10) Golub, E.; Pelossof, G.; Freeman, R.; Zhang, H.; Willner, I. Electrochemical, Photoelectrochemical, and Surface Plasmon Resonance Detection of Cocaine Using Supramolecular Aptamer Complexes and Metallic or Semiconductor Nanoparticles. *Anal. Chem.* **2009**, *81* (22), 9291−9298.

(11) Devadoss, A.; Sudhagar, P.; Terashima, C.; Nakata, K.; Fujishima, A. Photoelectrochemical Biosensors: New Insights into Promising Photoelectrodes and Signal Amplification Strategies. *J. Photochem. Photobiol., C* **2015**, *24*, 43−63.

(12) Sakib, S.; Pandey, R.; Soleymani, L.; Zhitomirsky, I. Surface Modification of TiO_2 for Photoelectrochemical DNA Biosensors. *Med. Devices Sensors* **2020**, *3* (2). DOI: 10.1002/mds3.10066.

(13) Victorious, A.; Clifford, A.; Saha, S.; Zhitomirsky, I.; Soleymani, L. Integrating TiO2 Nanoparticles within a Catecholic Polymeric Network Enhances the Photoelectrochemical Response of Biosensors. *J. Phys. Chem. C* **2019**, *123* (26), 16186−16193.

(14) Fan, G. C.; Ren, X. L.; Zhu, C.; Zhang, J. R.; Zhu, J. J. A New Signal Amplification Strategy of Photoelectrochemical Immunoassay for Highly Sensitive Interleukin-6 Detection Based on TiO2/CdS/CdSe Dual Co-Sensitized Structure. *Biosens. Bioelectron.* **2014**, *59*, 45−53.

(15) Huo, X.; Liu, P.; Zhu, J.; Liu, X.; Ju, H. Electrochemical Immunosensor Constructed Using TiO2 Nanotubes as Immobilization Scaffold and Tracing Tag. *Biosens. Bioelectron.* **2016**, *85*, 698−706.

(16) Yang, W.; Xu, W.; Wang, Y.; Chen, D.; Wang, X.; Cao, Y.; Wu, Q.; Tu, J.; Zhen, C. Photoelectrochemical Glucose Biosensor Based on the Heterogeneous Facets of Nanocrystalline TiO 2 /Au/Glucose Oxidase Films. *ACS Appl. Nano Mater.* **2020**, *3* (3), 2723−2732.

(17) Saha, S.; Victorious, A.; Pandey, R.; Clifford, A.; Zhitomirsky, I.; Soleymani, L. Differential Photoelectrochemical Biosensing Using DNA Nanospacers to Modulate Electron Transfer between Metal and Semiconductor Nanoparticles. *ACS Appl. Mater. Interfaces* **2020**, *12* (33), 36895−36905.

(18) Shen, S.; Chen, J.; Wang, M.; Sheng, X.; Chen, X.; Feng, X.; Mao, S. S. Titanium Dioxide Nanostructures for Photoelectrochemical Applications. *Prog. Mater. Sci.* **2018**, *98*, 299−385.

(19) Fujishima, A.; Rao, T. N.; Tryk, D. A. Titanium Dioxide Photocatalysts. *J. Photochem. Photobiol., C* **2000**, *1*, 1−21.

(20) Clavero, C. Plasmon-Induced Hot-Electron Generation at Nanoparticle/Metal-Oxide Interfaces for Photovoltaic and Photocatalytic Devices. *Nat. Photonics* **2014**, *8* (2), 95−103.
(21) Zhou, H.; Liu, J.; Zhang, S. Quantum Dot-Based Photoelectric Conversion for Biosensing Applications. *TrAC, Trends Anal. Chem.* **2015**, *67*, 56−73.
(22) Li, J.; Wu, N. Semiconductor-Based Photocatalysts and Photoelectrochemical Cells for Soalr Fuel Generation: A Review. *Catal. Sci. Technol.* **2015**, *5* (3), 1360−1384.
(23) Richhariya, G.; Kumar, A.; Tekasakul, P.; Gupta, B. Natural Dyes for Dye Sensitized Solar Cell: A Review. *Renewable and Sustainable Energy Reviews*; Elsevier, Ltd.: Amsterdam, March 1, 2017; pp 705−718 DOI: 10.1016/j.rser.2016.11.198.
(24) Ata, M. S.; Liu, Y.; Zhitomirsky, I. A Review of New Methods of Surface Chemical Modification, Dispersion and Electrophoretic Deposition of Metal Oxide Particles. *RSC Adv.* **2014**, *4* (43), 22716−22732.
(25) Zhang, T.; Wojtal, P.; Rubel, O.; Zhitomirsky, I. Density Functional Theory and Experimental Studies of Caffeic Acid Adsorption on Zinc Oxide and Titanium Dioxide Nanoparticles. *RSC Adv.* **2015**, *5* (129), 106877−106885.
(26) Li, J.; Wu, N. Semiconductor-Based Photocatalysts and Photoelectrochemical Cells for Solar Fuel Generation: A Review. *Catal. Sci. Technol.* **2015**, *5* (3), 1360−1384.
(27) Devan, R. S.; Patil, R. A.; Lin, J. H.; Ma, Y. R. One-Dimensional Metal-Oxide Nanostructures: Recent Developments in Synthesis, Characterization, and Applications. *Adv. Funct. Mater.* **2012**, *22* (16), 3326−3370.
(28) Ata, M. S.; Liu, Y.; Zhitomirsky, I. A Review of New Methods of Surface Chemical Modification, Dispersion and Electrophoretic Deposition of Metal Oxide Particles. *RSC Adv.* **2014**, *4* (43), 22716.
(29) Wu, K.; Wang, Y.; Zhitomirsky, I. Electrophoretic Deposition of TiO2 and Composite TiO2-MnO2 Films Using Benzoic Acid and Phenolic Molecules as Charging Additives. *J. Colloid Interface Sci.* **2010**, *352* (2), 371−378.
(30) Orchard, K. L.; Hojo, D.; Sokol, K. P.; Chan, M. J.; Asao, N.; Adschiri, T.; Reisner, E. Catechol-TiO2 Hybrids for Photocatalytic H2 Production and Photocathode Assembly. *Chem. Commun.* **2017**, *53* (94), 12638−12641.
(31) An, B. K.; Hu, W.; Burn, P. L.; Meredith, P. New Type II Catechol-Thiophene Sensitizers for Dye-Sensitized Solar Cells. *J. Phys. Chem. C* **2010**, *114* (41), 17964−17974.
(32) Tachan, Z.; Hod, I.; Zaban, A. The TiO_2-Catechol Complex: Coupling Type II Sensitization with Efficient Catalysis of Water Oxidation. *Adv. Energy Mater.* **2014**, *4* (6), 1301249.
(33) Higashimoto, S.; Nishi, T.; Yasukawa, M.; Azuma, M.; Sakata, Y.; Kobayashi, H. Photocatalysis of Titanium Dioxide Modified by Catechol-Type Interfacial Surface Complexes (ISC) with Different Substituted Groups. *J. Catal.* **2015**, *329*, 286−290.
(34) Eda, T.; Fujisawa, J. I.; Hanaya, M. Inorganic Control of Interfacial Charge-Transfer Transitions in Catechol-Functionalized Titanium Oxides Using SrTiO3, BaTiO3, and TiO2. *J. Phys. Chem. C* **2018**, *122* (28), 16216−16220.
(35) Finkelstein-Shapiro, D.; Davidowski, S. K.; Lee, P. B.; Guo, C.; Holland, G. P.; Rajh, T.; Gray, K. A.; Yarger, J. L.; Calatayud, M. Direct Evidence of Chelated Geometry of Catechol on TiO2 by a Combined Solid-State NMR and DFT Study. *J. Phys. Chem. C* **2016**, *120* (41), 23625−23630.
(36) Savić, T. D.; Čomor, M. I.; Nedeljković, J. M.; Veljković, D.; Zarić, S. D.; Rakić, V. M.; Janković, I. A. The Effect of Substituents on the Surface Modification of Anatase Nanoparticles with Catecholate-Type Ligands: A Combined DFT and Experimental Study. *Phys. Chem. Chem. Phys.* **2014**, *16* (38), 20796−20805.
(37) Abugazleh, M. K.; Rougeau, B.; Ali, H. Adsorption of Catechol and Hydroquinone on Titanium Oxide and Iron (III) Oxide. *J. Environ. Chem. Eng.* **2020**, *8* (5), 104180.
(38) Kim, J. H.; Joshi, M. K.; Lee, J.; Park, C. H.; Kim, C. S. Polydopamine-Assisted Immobilization of Hierarchical Zinc Oxide Nanostructures on Electrospun Nanofibrous Membrane for Photocatalysis and Antimicrobial Activity. *J. Colloid Interface Sci.* **2018**, *513*, 566−574.
(39) Yu, Z.; Zeng, H.; Min, X.; Zhu, X. High-Performance Composite Photocatalytic Membrane Based on Titanium Dioxide Nanowire/Graphene Oxide for Water Treatment. *J. Appl. Polym. Sci.* **2020**, *137* (12), 48488.
(40) Khan, M. A.; Mujahid, M. Recent Advances in Electrochemical and Optical Biosensors Designed for Detection of Interleukin 6. *Sensors (Switzerland)* **2020**, *20* (3), 646 DOI: 10.3390/s20030646.
(41) Huang, J.; Harvey, J.; Derrick Fam, W. H.; Nimmo, M. A.; Alfred Tok, I. Y. Novel Biosensor for Interleukin-6 Detection. *Procedia Eng.* **2013**, *60*, 195−200, DOI: 10.1016/j.proeng.2013.07.042.
(42) Wang, G.; He, X.; Chen, L.; Zhu, Y.; Zhang, X. Ultrasensitive IL-6 Electrochemical Immunosensor Based on Au Nanoparticles-Graphene-Silica Biointerface. *Colloids Surf., B* **2014**, *116*, 714−719.
(43) Syres, K. L.; Thomas, A. G.; Flavell, W. R.; Spencer, B. F.; Bondino, F.; Malvestuto, M.; Preobrajenski, A.; Grätzel, M. Adsorbate-Induced Modification of Surface Electronic Structure: Pyrocatechol Adsorption on the Anatase TiO 2 (101) and Rutile TiO 2 (110) Surfaces. *J. Phys. Chem. C* **2012**, *116* (44), 23515−23525.
(44) Li, S. C.; Wang, J. G.; Jacobson, P.; Gong, X. Q.; Selloni, A.; Diebold, U. Correlation between Bonding Geometry and Band Gap States at Organic-Inorganic Interfaces: Catechol on Rutile TiO 2(110). *J. Am. Chem. Soc.* **2009**, *131* (3), 980−984.
(45) Gulley-Stahl, H.; Hogan, P. A.; Schmidt, W. L.; Wall, S. J.; Buhrlage, A.; Bullen, H. A. Surface Complexation of Catechol to Metal Oxides: An ATR-FTIR, Adsorption, and Dissolution Study. *Environ. Sci. Technol.* **2010**, *44* (11), 4116−4121.
(46) Zhou, W.; Liu, X.; Cui, J.; Liu, D.; Li, J.; Jiang, H.; Wang, J.; Liu, H. Control Synthesis of Rutile TiO2Microspheres, Nanoflowers, Nanotrees and Nanobelts via Acid-Hydrothermal Method and Their Optical Properties. *CrystEngComm* **2011**, *13*, 4557−4563.
(47) Wang, X.; Li, Z.; Shi, J.; Yu, Y. One-Dimensional Titanium Dioxide Nanomaterials: Nanowires, Nanorods, and Nanobelts. *Chem. Rev.* **2014**, *114*, 9346−9384.
(48) Zander, Z.; Yagloski, R.; DeCoste, J.; Zhang, D.; DeLacy, B. G. One-Pot Synthesis of High Aspect Ratio Titanium Dioxide Nanorods Using Oxalic Acid as a Complexing Agent. *Mater. Lett.* **2016**, *163*, 39−42.
(49) Jun, Y.; Casula, M. F.; Sim, J.; Kim, S. Y.; Cheon, J.; Alivisatos, A. P. *J. Am. Chem. Soc.* **2003**, *125* (12), 15981−15985.
(50) Rangan, S.; Theisen, J. P.; Bersch, E.; Bartynski, R. A. Energy Level Alignment of Catechol Molecular Orbitals on ZnO(110) and TiO2 (110) Surfaces. *Appl. Surf. Sci.* **2010**, *256* (15), 4829−4833.
(51) Rajh, T.; Chen, L. X.; Lukas, K.; Liu, T.; Thurnauer, M. C.; Tiede, D. M. Surface Restructuring of Nanoparticles: An Efficient Route for Ligand-Metal Oxide Crosstalk. *J. Phys. Chem. B* **2002**, *106* (41), 10543−10552.
(52) Hodes, G. Photoelectrochemical Cell Measurements: Getting the Basics Right. *J. Phys. Chem. Lett.* **2012**, *3* (9), 1208−1213.
(53) Fan, D.; Wu, D.; Cui, J.; Chen, Y.; Ma, H.; Liu, Y.; Wei, Q.; Du, B. An Ultrasensitive Label-Free Immunosensor Based on CdS Sensitized Fe-TiO2 with High Visible-Light Photoelectrochemical Activity. *Biosens. Bioelectron.* **2015**, *74*, 843−848.
(54) Sarkar, S.; Makhal, A.; Lakshman, K.; Bora, T.; Dutta, J.; Kumar Pal, S. Dual-Sensitization via Electron and Energy Harvesting in CdTe Quantum Dots Decorated ZnO Nanorod-Based Dye-Sensitized Solar Cells. *J. Phys. Chem. C* **2012**, *116* (27), 14248−14256.
(55) Su, R.; Bechstein, R.; Sø, L.; Vang, R. T.; Sillassen, M.; Esbjörnsson, B.; Palmqvist, A.; Besenbacher, F. How the Anatase-to-Rutile Ratio Influences the Photoreactivity of TiO 2. *J. Phys. Chem. C* **2011**, *115* (49), 24287−24292.
(56) Swierk, J. R.; Regan, K. P.; Jiang, J.; Brudvig, G. W.; Schmuttenmaer, C. A. Rutile TiO 2 as an Anode Material for Water-Splitting Dye-Sensitized Photoelectrochemical Cells. *ACS Energy Lett.* **2016**, *1* (3), 603−606.
(57) Cho, I. S.; Chen, Z.; Forman, A. J.; Kim, D. R.; Rao, P. M.; Jaramillo, T. F.; Zheng, X. Branched TiO2 Nanorods for Photo-

electrochemical Hydrogen Production. *Nano Lett.* **2011**, *11*, 4978−4984.
(58) Han, Z.; Luo, M.; Chen, L.; Pan, H.; Chen, J.; Li, C. A Photoelectrochemical Biosensor for Determination of DNA Based on Flower Rod-like Zinc Oxide Heterostructures. *Microchim. Acta* **2017**, *184* (8), 2541−2549.
(59) Çakıroğlu, B.; Özacar, M. A Photoelectrochemical Biosensor Fabricated Using Hierarchically Structured Gold Nanoparticle and MoS2 on Tannic Acid Templated Mesoporous TiO2. *Electroanalysis* **2020**, *32* (1), 166−177.
(60) Qiu, Z.; Tang, D. Nanostructure-Based Photoelectrochemical Sensing Platforms for Biomedical Applications. *J. Mater. Chem. B* **2020**, *8* (13), 2541−2561.
(61) Lindgren, T.; Wang, H.; Beermann, N.; Vayssieres, L.; Hagfeldt, A.; Lindquist, S. Aqueous Photoelectrochemistry of Hematite Nanorod Array. *Sol. Energy Mater. Sol. Cells* **2002**, *71*, 231−243.
(62) Pandey, R.; Chang, D.; Smieja, M.; Hoare, T.; Li, Y.; Soleymani, L. Integrating Programmable DNAzymes with Electrical Readout for Rapid and Culture-Free Bacterial Detection Using a Handheld Platform. *Nat. Chem.* **2021**, *13*, 895.
(63) Woo, S. M.; Gabardo, C. M.; Soleymani, L. Prototyping of Wrinkled Nano-/Microstructured Electrodes for Electrochemical DNA Detection. *Anal. Chem.* **2014**, *86* (24), 12341−12347.
(64) Saha, S.; Chan, Y.; Soleymani, L. Enhancing the Photoelectrochemical Response of DNA Biosensors Using Wrinkled Interfaces. *ACS Appl. Mater. Interfaces* **2018**, *10* (37), 31178−31185.
(65) Liu, A.; Yin, K.; Mi, L.; Ma, M.; Liu, Y.; Li, Y.; Wei, W.; Zhang, Y.; Liu, S. A Novel Photoelectrochemical Immunosensor by Integration of Nanobody and ZnO Nanorods for Sensitive Detection of Nucleoside Diphosphatase Kinase-A. *Anal. Chim. Acta* **2017**, *973*, 82−90.
(66) Li, H.; Li, Z.; Yu, Y.; Ma, Y.; Yang, W.; Wang, F.; Yin, X.; Wang, X. Surface Plasmon Resonance Enhanced Photoelectrochemical Water Splitting from Au Nanoparticle-Decorated 3D TiO Nanorod Architectures Surface Plasmon Resonance Enhanced Photoelectrochemical Water Splitting from Au Nanoparticle-Decorated 3D TiO_2 Nanorod Arc. *J. Phys. Chem. C* **2017**, *121* (22), 12071−12079.
(67) Zhao, W. W.; Shan, S.; Ma, Z. Y.; Wan, L. N.; Xu, J. J.; Chen, H. Y. Acetylcholine Esterase Antibodies on BiOI Nanoflakes/TiO2 Nanoparticles Electrode: A Case of Application for General Photoelectrochemical Enzymatic Analysis. *Anal. Chem.* **2013**, *85* (24), 11686−11690.
(68) Li, J.; Li, H.; Xue, Y.; Fang, H.; Wang, W. Facile Electrodeposition of Environment-Friendly Cu2O/ZnO Heterojunction for Robust Photoelectrochemical Biosensing. *Sens. Actuators, B* **2014**, *191*, 619−624.
(69) Li, W.; Sheng, P.; Cai, J.; Feng, H.; Cai, Q. Highly Sensitive and Selective Photoelectrochemical Biosensor Platform for Polybrominated Diphenyl Ether Detection Using the Quantum Dots Sensitized Three-Dimensional, Macroporous ZnO Nanosheet Photoelectrode. *Biosens. Bioelectron.* **2014**, *61*, 209−214.
(70) Yan, Z.; Wang, Z.; Miao, Z.; Liu, Y. Dye-Sensitized and Localized Surface Plasmon Resonance Enhanced Visible-Light Photoelectrochemical Biosensors for Highly Sensitive Analysis of Protein Kinase Activity. *Anal. Chem.* **2016**, *88* (1), 922−929.
(71) Liu, X.-P.; Xie, X.-L.; Wei, Y.-P.; Mao, C.-j.; Chen, J.-S.; Niu, H.-L.; Song, J.-M.; Jin, B.-K. Photoelectrochemical Immunoassay for Human Interleukin 6 Based on the Use of Perovskite-Type LaFeO3 Nanoparticles on Fluorine-Doped Tin Oxide Glass. *Microchim. Acta* **2018**, *185* (1), 1−6.
(72) Aydin, S. A Short History, Principles, and Types of ELISA, and Our Laboratory Experience with Peptide/Protein Analyses Using ELISA. *Peptides* **2015**, *72*, 4−15.
(73) Cinquanta, L.; Fontana, D. E.; Bizzaro, N. Chemiluminescent Immunoassay Technology: What Does It Change in Autoantibody Detection? *Autoimmun. Highlights* **2017**, *8* (1). DOI: 10.1007/s13317-017-0097-2.
(74) Zanut, A.; Fiorani, A.; Canola, S.; Saito, T.; Ziebart, N.; Rapino, S.; Rebeccani, S.; Barbon, A.; Irie, T.; Josel, H. P.; Negri, F.; Marcaccio, M.; Windfuhr, M.; Imai, K.; Valenti, G.; Paolucci, F. Insights into the Mechanism of Coreactant Electrochemiluminescence Facilitating Enhanced Bioanalytical Performance. *Nat. Commun.* **2020**, *11* (1), 1−9.
(75) Thiha, A.; Ibrahim, F. A Colorimetric Enzyme-Linked Immunosorbent Assay (ELISA) Detection Platform for a Point-of-Care Dengue Detection System on a Lab-on-Compact-Disc. *Sensors* **2015**, *15* (5), 11431−11441.

https://doi.org/10.1021/acsami.1c18240
ACS Appl. Mater. Interfaces 2021, 13, 50851−50861